

The Discovery of the Long-Period, Eccentric Planet Kepler-88 d and System Characterization with Radial Velocities and Photodynamical Analysis

LAUREN M. WEISS,¹ ERIC AGOL,² DANIEL C. FABRYCKY,³ SEAN M. MILLS,⁴ ANDREW W. HOWARD,⁵
HOWARD ISAACSON,⁶ ERIK A PETIGURA,⁷ BENJAMIN FULTON,⁸ LEA HIRSCH,⁹ EVAN SINUKOFF,⁴

¹*Institute for Astronomy, 2680 Woodlawn Dr., Honolulu, HI 96822, USA*

²*Department of Astronomy, University of Washington, Seattle, WA*

³*Department of Astronomy and Astrophysics, University of Chicago, 5640 S. Ellis Ave, Chicago, IL 60637, USA*

⁴*California Institute of Technology, 1200 E California Blvd, Pasadena, CA 91125, USA*

⁵*California Institute of Technology, Pasadena, CA 91125, USA*

⁶*501 Campbell Hall, University of California at Berkeley, Berkeley, CA 94720, USA*

⁷*Department of Physics & Astronomy, University of California Los Angeles, Los Angeles, CA 90095, USA*

⁸*NASA Exoplanet Science Institute, MC 314-6, 1200 E California Blvd, Pasadena, CA 91125, USA*

⁹*Varian Physics, Room 108, 382 Via Pueblo Mall, Stanford, CA 94305, USA*

ABSTRACT

We present the discovery of Kepler-88 d ($P_d = 1414^{+27}_{-23}$ days, $M \sin i_d = 959 \pm 57 M_\oplus$, $e_d = 0.432 \pm 0.048$) based on six years of radial velocity (RV) follow-up from the W. M. Keck Observatory HIRES spectrograph. Kepler-88 has two previously identified planets: Kepler-88 b (KOI-142.01) transits in the NASA *Kepler* photometry and has very large transit timing variations. Nesvorný et al. (2013) performed a dynamical analysis of the TTVs to uniquely identify the orbital period and mass of the perturbing planet (Kepler-88 c), which was later confirmed with RVs from the Observatoire Haute-Provence (OHP, Barros et al. 2014). To fully explore the architecture of this system, we performed photodynamical modeling on the *Kepler* photometry combined with the RVs from Keck and OHP and stellar parameters from spectroscopy and Gaia. Planet d is not detectable in the photometry, and long-baseline RVs are needed to ascertain its presence. However, the orbital parameters and masses of interacting planets b and c are improved by an order of magnitude with respect to the RV-only solution when the photometry is included: $P_b = 10.91647 \pm 0.00014$ days, $M_b = 9.5 \pm 1.2 M_\oplus$, $P_c = 22.2649 \pm 0.0007$ days, and $M_c = 214.2 \pm 5.2 M_\oplus$. The photodynamical solution also finds that planets b and c have low eccentricities, are apsidally anti-aligned, and have conjunctions on the same hemisphere of the star. Continued RV follow-up of systems with small planets will improve our understanding of the link between inner planetary system architectures and giant planets.

1. INTRODUCTION

The NASA *Kepler* Mission detected hundreds of systems with multiple transiting planets (Lissauer et al. 2011; Fabrycky et al. 2014; Rowe et al. 2014; Lissauer et al. 2011), providing insight into one of the most common modes of

planet formation. One unexpected attribute of the *Kepler* planetary systems is that planets in or very near mean-motion resonances are rare (Fabrycky et al. 2014). The prevalence of planets that are not mean-motion resonances seems at odds with examples from our solar system

(e.g., the Galilean moons) and resonant chains of giant exoplanets detected in radial velocity surveys (e.g., [Marcy et al. 2001](#)). One explanation for resonant architectures is that planet pairs migrating convergently become trapped in the energetically favorable configuration of mean motion resonance.

Kepler-88 (KOI-142) is a rare example of a planetary system very near a mean-motion resonance. The system has only one transiting planet, Kepler-88 b (KOI-142.01), a sub-Neptune-sized planet with orbital period of 10.95 days. Kepler-88 b is perturbed by a non-transiting giant planet with a period of 22.25 days, Kepler-88 c (KOI-142.02, [Nesvorný et al. 2013](#)). The resonant conjunctions of the sub-Neptune and giant planet produce large transit timing variations (TTVs), which have an amplitude of half a day (5% of the orbital period of the transiting planet, see [Figure 1](#)). These very large TTVs led to the nickname “The King of TTVs” for the Kepler-88 system ([Steffen et al. 2012a](#)) and have been identified in various TTV catalogs (e.g., [Ford et al. 2011](#); [Steffen et al. 2012a](#)) and have been identified in various TTV catalogs (e.g., [Ford et al. 2011](#); [Steffen et al. 2012a](#); [Mazeh et al. 2013](#); [Holczer et al. 2016](#)).

The Kepler-88 b TTVs were first explained dynamically in [Nesvorný et al. \(2013, N13\)](#). In a forward-modeled N-body dynamical fit, they found that (1) the perturber of the Neptune-sized planet is at $22.3397^{+0.0021}_{-0.0018}$ days, (2), the mass of the perturber is $198.8^{+9.2}_{-10.6} M_{\oplus}$, (3) the eccentricities of the 11-day and 22-day planet are small but non-zero ($e_b = 0.05596^{+0.00048}_{-0.00034}$, $e_c = 0.0567^{+0.0010}_{-0.0013}$), and (4) the orbits of the resonant planets are apsidally anti-aligned ($\Delta\varpi = 180 \pm 2^\circ$). N13 also found non-negligible transit duration variations (TDVs) of the transiting planet, which provided a constraint on the mutual inclination of the two planets.

Shortly thereafter, [Barros et al. \(2014\)](#) used the Observatoire Haute Provence (OHP) telescope and SOPHIE high-resolution echelle spectrograph to measure radial velocities (RVs) of

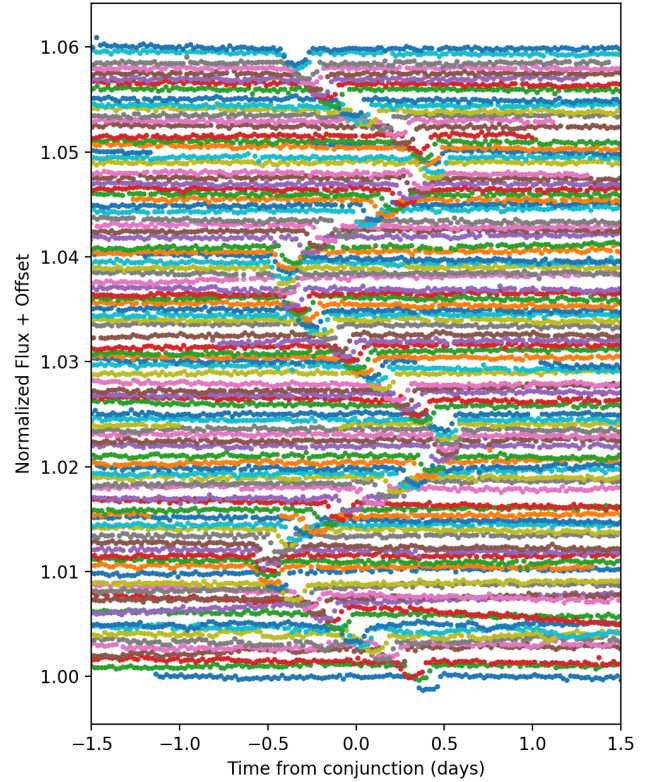


Figure 1. The Kepler long-cadence photometry of Kepler-88 near expected times of conjunction for Kepler-88 b ($P = 10.95$ days), with individual transits offset vertically (epoch increases from bottom to top). The TTVs of amplitude 0.5 days are readily identifiable.

the Kepler-88 system. With one season of RVs, they confirmed the presence of a $241^{+102}_{-51} M_{\oplus}$ planet with an orbital period of 22.10 ± 0.25 days. This was the first time that RVs confirmed an accurate and precise prediction of the location and mass of a non-transiting exoplanet from TTVs.

In this paper, we present RVs of Kepler-88 from the W. M. Keck Observatory HIRES spectrograph taken between the years 2013 and 2019. Our RVs confirm the existence, mass, and orbital period of the giant planet at 22.26 days. We also detect another giant planet in

the system, Kepler-88 d, at an orbital period of 1414_{-23}^{+27} days, with $M \sin i_d$ of $959 \pm 57 M_{\oplus}$ and an eccentricity of 0.432 ± 0.048 . The high mass and eccentricity of Kepler-88 d indicate that it has likely been an important dynamical component in this planetary system’s history. To identify accurate dynamical parameters for all of the known bodies in the system, we simultaneously forward-model the Kepler photometry, Keck-HIRES RVs, and OHP-SOPHIE RVs of Kepler-88 with multiple N-body codes.

This paper is organized as follows: In §2, we present our observing strategy and the Keck-HIRES RVs, literature RVs, and stellar properties. In the following sections, we explore the RV data with increasingly complex models and supplementary data. In §3, we present a three-planet Keplerian model to the RVs. In §4, we present the results of a simultaneous N-body fit to the RVs and TTVs. In §5, we perform simultaneously an N-body fit to the RVs and *Kepler* photometry (a photodynamical fit). In §6, we present the main results from our analyses. In §7, we discuss how our results affect our interpretation of the history of this planetary system, and how this system adds to the small but growing list of systems with characterizations from both RV and TTV analyses. In §8 we conclude.

2. KECK-HIRES SPECTRA

2.1. Radial Velocities

We obtained 40 RVs of Kepler-88 on the HIRES spectrograph (Vogt et al. 1994) at the W. M. Keck Observatory between the years 2013 and 2019. We used the standard HIRES setup of the California Planet Search (see Howard et al. 2010, for details). Spectra were obtained using HIRES in the red-collimation mode with a warm molecular iodine gas cell in the light path for wavelength calibration. We used the C2 decker ($0.''86 \times 14''$, $R=60,000$) to enable sky-subtraction for this relatively faint ($V = 13.8$) target. Since the target was faint,

Table 1. Kepler-88 RVs

Time (BJD - 2454900)	RV (m/s)	σ_{RV} (m/s)	S_{HK}	Inst
1575.0479080001824	-33.19	2.79	HIRES	
1575.4094699998386	42.0	10.0	SOPHIE	
1575.9926950000226	-34.06	2.32	HIRES	
1577.8927310002036	-50.64	2.50	HIRES	
1579.0270790001377	-79.66	2.63	HIRES	
...

NOTE—Times are in BJD - 2454900.0. SOPHIE RVs are from Barros et al. (2014); HIRES RVs are from this work. The SOPHIE RVs have had 20465.0 m s^{-1} added for easier zero-point calibration. The RV uncertainties do not include RV jitter. The full table is available in machine readable form. The first few lines are shown here for content and format.

we only observed in good conditions (seeing $< 1.''5$, clear to thin clouds). For each spectrum, we achieved a signal to noise ratio of at least 50 to ensure that our Doppler pipeline would deliver RVs with errors of $< 10 \text{ m s}^{-1}$ (Howard & Fulton 2016).

We observed an iodine-free template spectrum bracketed by observations of rapidly rotating B-type stars to enable a deconvolution of the stellar spectrum from the spectrograph PSF. We then forward-modeled our RV spectra with the deconvolved template stellar spectrum plus a night-specific model of our PSF convolved with an atlas iodine spectrum. We also used the blue HIRES chip to extract a Mt. Wilson S_{HK} value for each HIRES observation. Our Keck-HIRES RVs and S_{HK} values, plus the SOPHIE RVs from the literature, are presented in Table 1.

2.2. Stellar Parameters

The stellar properties of Kepler-88 were determined based on our high signal-to-noise template spectrum in combination with the *Gaia* parallax and 2MASS photometry (Fulton & Pe-

figura 2018). The star has a similar mass to the sun, but is enhanced in metals ($M_{\star} = 0.985_{-0.022}^{+0.027} M_{\odot}$, $[\text{Fe}/\text{H}] = 0.27 \pm 0.06$). Kepler-88 is slightly smaller than the sun ($R_{\star} = 0.900 \pm 0.022 R_{\odot}$).

Because the transit of planet b combined with dynamical information about the planet constrains the density of the star, we used a photodynamical fit to update the stellar characterization (e.g., Vanderburg et al. 2017, see section 5.2). We used the best-fit values and uncertainties for the stellar mass and radius from Fulton & Petigura (2018) as priors in our photodynamical fit. After our photodynamical fit, the best-fit stellar mass and radius are $M_{\star} = 0.99 \pm 0.024 M_{\odot}$ and $R_{\star} = 0.897 \pm 0.016 R_{\odot}$. The precision of the stellar radius determination was improved through the photodynamical fit, suggesting that the transits provide information about the stellar density and hence the stellar radius.¹

Of the stellar parameters reported here, only the stellar mass is dependent on isochrone fitting (see Fulton & Petigura 2018, for details). We caution that the formal error in the mass reported here does not account for systematic differences between the stellar isochrones formulated by different research groups, and so the reported error in the stellar mass (and hence density) might be underestimated.

3. KEPLERIAN FIT

The RVs of Kepler-88 show long-term variation from a planetary companion at ~ 4 years (see Figures 2, 3, and 4). The discovery of this companion is the result of the long baseline (currently six years) of Keck-HIRES RVs. The 4-year RV variation does not correlate with S_{HK} variability, strongly disfavoring a stellar activity cycle as the source of the RV signal.

¹ The stellar mass was essentially unchanged, which is the expected behavior from Phodymm (Mills et al. 2016).

To obtain initial estimates of the orbital properties of all three planets, we fit the RVs from both HIRES and SOPHIE with a 3-planet Keplerian model. Since the innermost planet is very low mass, we fixed its orbital period and transit time at the best linear-ephemeris values as determined from the Holczer et al. (2016) TTVs, and kept its eccentricity fixed. We allowed the five orbital elements P , T_p , $\sqrt{e}\cos\omega$, $\sqrt{e}\sin\omega$, and K to vary for planets c and d, as well the HIRES RV zeropoint (γ_{HIRES}), the SOPHIE RV zeropoint (γ_{SOPHIE}), and the RV jitter for each telescope (σ_{HIRES}), (σ_{SOPHIE}). Our priors were $0 < e < 1$ and $K > 0$ for all planets. We explored these parameters with a Markov-Chain Monte Carlo (MCMC) analysis, the results of which are in Tables 2 and 3.

The RVs place tight constraints on planet masses $M \sin i_c$ ($206.7 \pm 12 M_{\oplus}$) and $M \sin i_d$ ($959 \pm 57 M_{\oplus}$), but provide very little information about M_b . This is because the transiting planet is small and the star is faint; many RVs are needed in this regime to obtain accurate and precise planet masses. As we show below, however, incorporating the TTVs or a full photodynamical model dramatically improves our constraint on the masses and orbits of Kepler-88 b and c with respect to the RV-only solution.

4. N-BODY FIT TO TTVS + RVs

A detailed N-body analysis is necessary to accurately model the positions and velocities of the Kepler-88 bodies because the two inner planets are near resonance. We used the N-body code TTVFast (Deck et al. 2014) to simultaneously reproduce the TTVs and RVs in the Kepler-88 system. For this analysis, we used the TTVs published in Holczer et al. (2016), which are measured from the *Kepler* long-cadence photometry. Our optimization algorithms included least-squares minimization and MCMC analysis. We considered a two-planet model (planets b and c only) and a three-planet model (planets b, c, and d), fitting the

Table 2. RV Only Keplerian MCMC Posteriors

Parameter	Credible Interval	Maximum Likelihood	Units
Orbital Parameters			
P_b	$\equiv 10.9531$	$\equiv 10.9531$	days
T_{conj_b}	$\equiv 175.1591$	$\equiv 175.1591$	BJD - BJD ₀
e_b	$\equiv 0.06$	$\equiv 0.06$	
ω_b	$\equiv -3.1306$	$\equiv -3.1306$	rad
K_b	$2.5^{+1.6}_{-1.4}$	2.6	m s ⁻¹
P_c	$22.2695^{+0.0046}_{-0.0044}$	22.2694	days
T_{conj_c}	$172.2^{+0.48}_{-0.5}$	172.19	BJD - BJD ₀
e_c	$0.027^{+0.029}_{-0.019}$	0.017	
ω_c	$-0.4^{+1.9}_{-1.5}$	-0.8	rad
K_c	$47.9^{+1.9}_{-1.8}$	47.9	m s ⁻¹
P_d	1421^{+27}_{-23}	1420	days
T_{conj_d}	1323^{+30}_{-33}	1324	BJD - BJD ₀
e_d	0.407 ± 0.042	0.404	
ω_d	$0.045^{+0.089}_{-0.086}$	0.036	rad
K_d	$60.5^{+4.5}_{-4.0}$	60.7	m s ⁻¹
Other Parameters			
γ_{SOPHIE}	$41.8^{+4.6}_{-4.8}$	42.2	m s ⁻¹
γ_{HIRES}	$-2.4^{+1.5}_{-1.6}$	-2.5	m s ⁻¹
$\dot{\gamma}$	$\equiv 0.0$	$\equiv 0.0$	
$\ddot{\gamma}$	$\equiv 0.0$	$\equiv 0.0$	
σ_{SOPHIE}	$8.7^{+5.4}_{-5.0}$	6.4	m s ⁻¹
σ_{HIRES}	$6.68^{+1.1}_{-0.91}$	5	m s ⁻¹

BJD₀ = 2454900.

TTVs alone, and then the RVs and TTVs simultaneously. We varied the masses, orbital periods, eccentricities and arguments of pericenter (via parameters $\sqrt{e}\cos\omega$ and $\sqrt{e}\sin\omega$), and mean anomalies for each of the planets at epoch BJD=2454954.62702, as well as the inclination and longitude of ascending node for planet c, and an RV zeropoint jitter for each spectrograph. We penalized high values of RV jitter in our minimization function χ'^2 :

$$\chi'^2 = \chi_{\text{RV}}^2 + \chi_{\text{TTV}}^2 + \sum_i 2\ln\sqrt{2\pi\sigma_i'^2}, \quad (1)$$

where σ_i' is the quadrature sum of the i th individual RV error and the RV jitter of the corresponding spectrograph, and χ^2 is the usual statistic

$$\chi^2 = \sum_i \frac{(x_{\text{meas},i} - x_{\text{mod},i})^2}{\sigma_i'^2}. \quad (2)$$

We compared the goodness of fit of our four models using the Bayesian Information Criterion (BIC):

$$\text{BIC} = \chi'^2 + \ln(N)N_{\text{varys}} \quad (3)$$

Table 3. RV-Only Keplerian Derived Posteriors

Parameter	Credible Interval	Maximum Likelihood	Units
$M_b \sin i$	$8.5^{+5.5}_{-4.9}$	10.6	M_{\oplus}
ρ_b	$0.85^{+0.71}_{-0.49}$	1.06	g cm^{-3}
a_b	$0.09604^{+0.00063}_{-0.00065}$	0.09646	AU
$M_c \sin i$	$0.657^{+0.028}_{-0.026}$	0.697	M_{Jup}
a_c	0.154 ± 0.001	0.155	AU
$M_d \sin i$	$3.03^{+0.19}_{-0.17}$	2.95	M_{Jup}
a_d	$2.464^{+0.035}_{-0.031}$	2.428	AU

where N is the number of data points (TTV alone or RV + TTV, depending on which data were used) and N_{varys} is the number of variables. Note that we use χ'^2 instead of χ^2 in calculating the BIC so that the penalty for large RV jitters is included in our model comparison. The χ^2 values, degrees of freedom, and BICs from our four-way analysis are summarized in Table 4. If only the TTVs are fit, a two-planet model is adequate for fitting the data, based on the similar values of the BIC for the two- and three-planet models ($\Delta\text{BIC}= 26$, in favor of the 2-planet model). However, in fitting the TTVs combined with the RVs, a three-planet model is strongly preferred, with $\Delta\text{BIC}= -120$. To illustrate the better performance of the three-planet model, the RVs are shown with our best two-planet fit (Figure 3) and our best three-planet fit (Figure 4). The TTVs and our best three-planet fit are shown in Figure 5. The best-fit planet masses and orbits from the TTV and TTV+RV analyses are within 1σ of the values we find in our photodynamical analysis, which is presented in §5.

5. PHOTODYNAMICAL FIT TO TRANSITS AND RVs

To improve upon the RV + TTV solution, we used a photodynamical forward-model to simultaneously fit the photometry and RVs of the Kepler-88 system. This allowed us to explore the inclinations of the planets, which can be

constrained by the transit depth and duration variations. We use the code `Phodymm` which has previously been used to fit photometry from the *Kepler* prime mission in Kepler-223, (Mills et al. 2016), Kepler-444 (Mills & Fabrycky 2017a) and Kepler-108 (Mills & Fabrycky 2017b), and the combined *Kepler* prime photometry and Keck-HIRES RVs in Kepler-25, Kepler-65, and Kepler-68 (Mills et al. 2019). `Phodymm` is a Runge-Kutta N-body integrator that can simultaneously forward-model photometry and RVs for N planets and one star. The transit shape is reproduced with the prescription given in Pál et al. (2011). This fit includes a transit shape described by Mandel & Agol (2002), with the quadratic limb-darkening coefficients of Claret (2000). For simplicity, `Phodymm` assumes that the velocity of the planet is constant during transit. For input parameters, it can accept Cartesian, astero-centric, or Jacobi coordinates. We used the Jacobi orbital elements: orbital period P , time of conjunction T_c , eccentricity e , inclination i , longitude of ascending node Ω , and argument of periastron passage ω all of which were defined at epoch $\text{BJD} = 2454954.62702$. Additional input parameters were the planet-to-star radius ratio R_p/R_* , and planet mass M_p for each planet, as well as the stellar mass M_* , radius R_* , dilution D , and quadratic limb-darkening coefficients c_1 and c_2 .

Table 4. Model Comparison

Model	Data	N_{varys}	χ_{TTV}^2	χ_{RV}^2	σ_{HIRES} (m s^{-1})	σ_{SOPHIE} (m s^{-1})	χ'^2	DOF	BIC
2 planets	TTVs	16	149.5	0	-	-	149.5	105	226.3
3 planets	TTVs	21	149.6	0	-	-	150.3	100	250.4
2 planets	TTVs + RVs	16	150.2	106.6	20.0	9.6	665.9	158	748.4
3 planets	TTVs + RVs	21	150.5	53.8	6.6	8.1	520.5	153	628.9
3 planets, control	Phot + RVs	26	-	73.0	6.7	6.1	1564293.6	1564456	1564664.4
3 planets, i_c flipped	Phot + RVs	26	-	45.5	6.5	9.4	1564330.4	1564456	1564701.2
3 planets, $i_d = 30^\circ$	Phot + RVs	26	-	75.6	6.7	6.1	1564298.0	1564456	1564668.8

NOTE—There are 121 TTV data, 53 RV data, and 1564429 photometric data. σ_{HIRES} and σ_{SOPHIE} are the HIRES and SOPHIE jitter terms, respectively, which are added to the intrinsic RV errors in quadrature.

5.1. Photometry

We downloaded the photometry of Kepler-88 (KOI-142, KIC 5446285) obtained during the Kepler prime mission from the MAST archive². Where available (quarters 4-17), we used short cadence data; we used long cadence data elsewhere. We detrended the photometry in the manner of Mills & Fabrycky (2017b). First, we segmented the lightcurve into chunks of approximately one day, masking any transits within each chunk. We then fit the photometry in each chunk with a cubic polynomial to model the continuum, including both systematic effects and stellar rotation.³ We divided the observed flux by our continuum model to obtain normalized photometry. We multiplied all the uncertainties by a scale factor such that the out of transit reduced chi square is 1.0, for both long cadence and short cadence independently. The detrended photometry is presented in Figure 6.

5.2. Photodynamical Fit

Since no stellar companions are known, we fixed the transit dilution at zero for all the planets, and we fixed planet-to-star radius ratios of the two non-transiting planets, the longitude of ascending node for planet b of $\Omega_b = 0.0$ (since this is an arbitrary angle on the sky plane), and the inclination and longitude of ascending node for planet d at $i_d = 89^\circ$, $\Omega_d = 0.0$ (the RVs only give $M \sin i$ information for this planet, and the TTVs do not help constrain its inclination). All other parameters were varied.

We arrived at our best estimate of the dynamical parameters in the following manner. First, we used the parameters published in N13 in conjunction with the software package *TTVFast* (Deck et al. 2014) to minimize our fit to the long-cadence determined TTVs reported in Holzer et al. (2016). When our fit to the long-cadence TTVs was optimized, we used our best fit as input orbital elements for *Phodymm*. We then ran 40 differential evolution MCMC (DE-MCMC) chains 10^6 steps each to obtain improved initial orbital elements and formal uncertainties. The chains were well-mixed based, on both a visual inspection of the chain for each parameter and a maximum Gelman-Rubin statistic of 1.05 (Gelman & Rubin 1992). Our best-fit parameters and uncertainties for the photo-

² <https://archive.stsci.edu/>

³ The anomaly at 180 days is a systematic discontinuity in the *Kepler* photometry that was not removed by our detrending algorithm. The artifact is not near any transits.

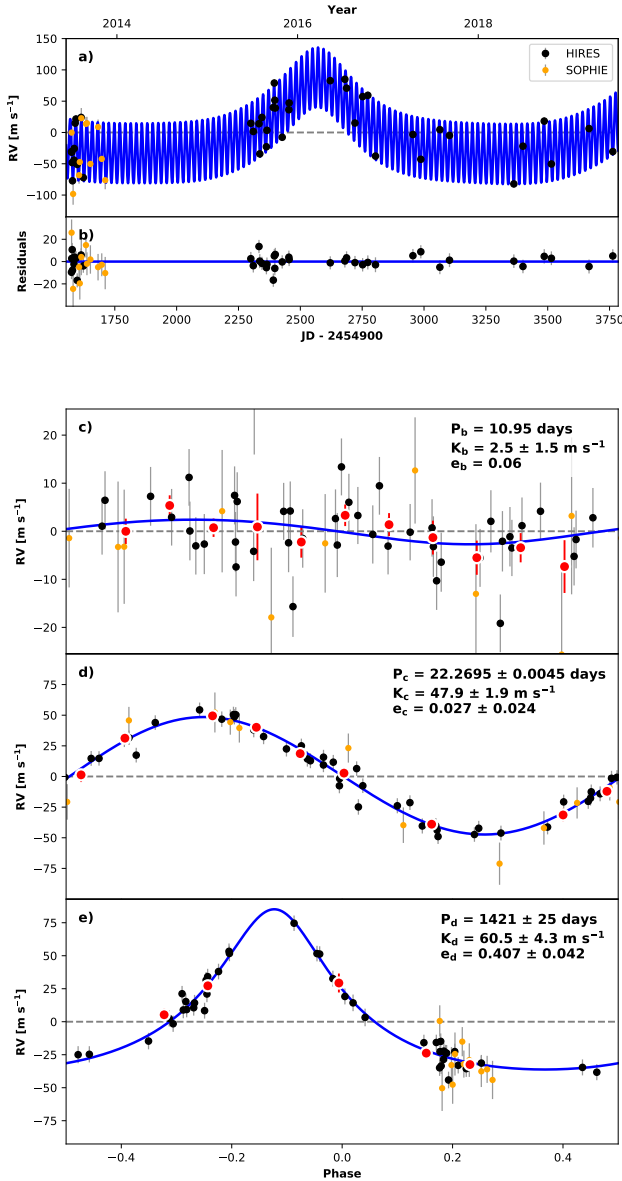


Figure 2. a: the RVs of Kepler-88 from Keck-HIRES (black) and OHP-SOPHIE (orange), and their errors (including jitter) as a function of time. The best fit 3-planet Keplerian solution is shown in blue. b: the residuals. c: The RVs phase-folded to the linear ephemeris of planet b, with the other Keplerian signals removed. The RVs alone do not detect the mass of planet b, but planet b clearly exists from its transits. d: Same as above, but for planet c, which does not transit. e: Same as above, but for planet d, which does not transit. With a period of 1414^{+27}_{-23} days, planet d is not detected in the TTVs, and so only the RVs provide a useful determination of its orbital properties.

dynamical N-body forward-model are in Table 5. Figure 6 shows the Q1-Q17 detrended *Kepler* photometry of Kepler-88, with our best photodynamical fit overplotted. Note that the residuals do not have strong correlated features, suggesting that the individual transit times, depths, shapes, and durations have been well-modeled.⁴ Figure 7 provides a zoom-in view from the middle of the short-cadence photometry, with colored marks at the top indicating the conjunction times for the planets. Figure 8 shows the photometry phase-folded to the individual transit times of Kepler-88 b. The sharp ingress and egress indicate that the individual transit times have been well-determined. Furthermore, the distribution of the photometric residuals during transit are identical to the distribution of the photometric residuals outside of transit, and both are Gaussian, with a standard deviation of 550 parts per million per exposure. No transits of planets c or d were detected.

5.3. Transit Times

One outcome of the photodynamical modeling is an improved determination of the individual transit times. The transit midpoints, impact parameters, and transit velocities for each transit epoch of Kepler-88 b are given in Table 6 from the date of the first *Kepler* transit through November 2022. The times of conjunction for each planet are shown as colored ticks in Figures 6 and 7: green for planet b, red for planet c, and yellow for planet c. Transits of planets c and d are not detected.

6. RESULTS

6.1. Confirmation of a giant planet near a 2:1 MMR

In both our RV-only and our photodynamical analysis, we confirm the existence of a giant

⁴ We tested this assertion by computing the auto-correlation function of the residuals, the magnitude of which did not exceed 0.002 for lags larger than unity.

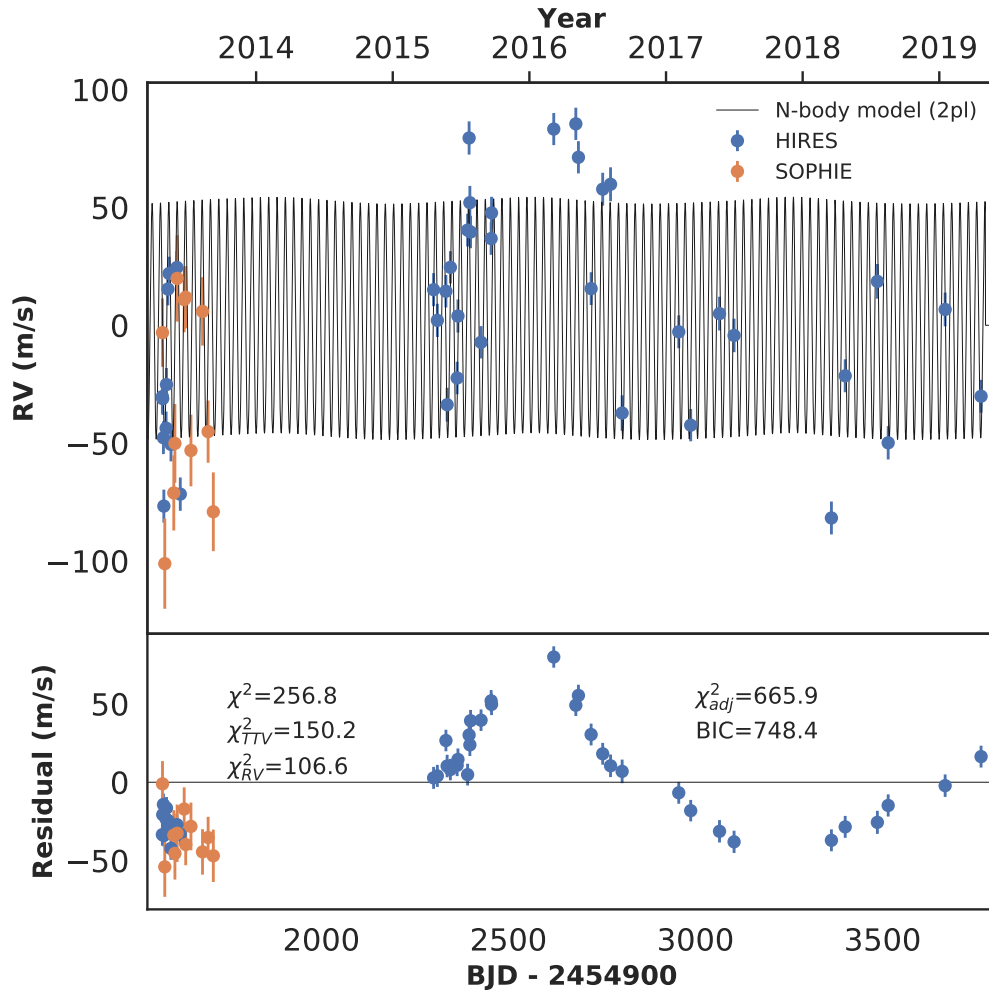


Figure 3. Top: Kepler-88 Radial velocities from Keck-HIRES (blue) and OHP-SOPHIE (orange). The best two-planet N-body fit to the RVs and TTVs (Kepler-88 b and c) is shown in black. Bottom: the RV residuals. There is a strong residual RV signal near 1414_{-23}^{+27} days. The χ^2 values of the fit to the TTVs and RVs are given, as is the penalty-adjusted $\chi^2 = \chi^2_{\text{P adj}}$ and BIC.

planet at 22.26 days with a mass of $200 M_{\oplus}$. A Lomb-Scargle periodogram of our RVs produces a very strong peak at 22.27 days, with no significant peaks at aliases or harmonics of this period, indicating that 22.27 days is in fact the period of the perturbing giant planet (Figure 9).

6.2. Discovery of a long-period giant planet

In the Keck-HIRES RV data, we identify a third planet at 1414_{-23}^{+27} days with $M_p \sin i = 959 \pm 57 M_{\oplus}$. When we compute the Lomb-Scargle periodogram to the residual RVs of a 2-planet fit (where the orbits are N-body), there is a significant peak at $P = 1413$ days,

and there are no other peaks with comparable power (see Figure 9). We find evidence for the third planet in the significantly improved χ^2 statistic to the RVs, which we summarize in Table 4. Without the third planet, our best N-body fit to the TTVs + RVs has $\chi^2_{\text{RV}} = 106.2$ (see Figure 3). Including the third planet near $P = 1413$ days results in $\chi^2_{\text{RV}} = 51.6$ (see Figure 4). The inclusion of the third planet substantially improves the fit to the RVs while simultaneously reducing the HIRES RV jitter by a factor of ~ 3 . However, the goodness of fit to the TTVs does not change significantly between the 2-planet and 3-planet models, indicating that

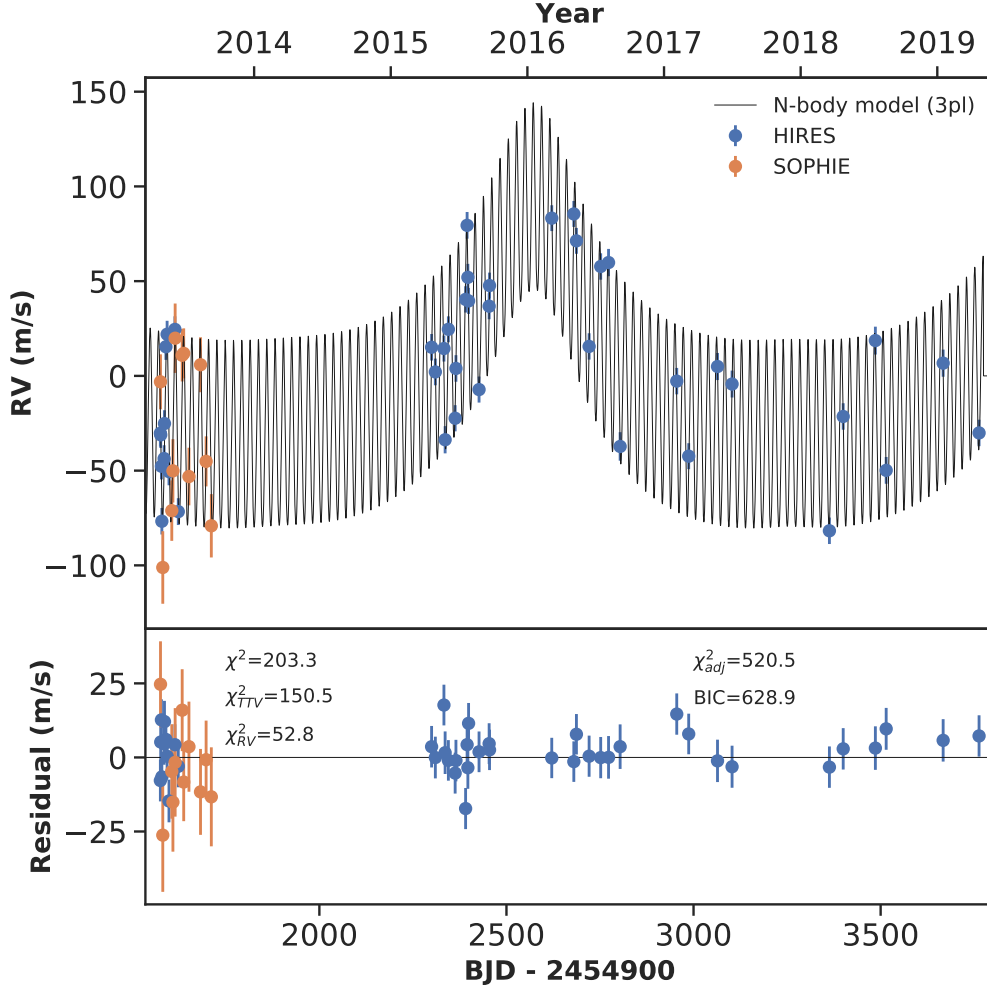


Figure 4. Same as Figure 3, but showing the best three-planet N-body model and residuals. The inclusion of the third planet substantially reduces the RV residuals and improves (reduces) the BIC.

the TTVs provide essentially no evidence for the existence of planet d. This is unsurprising, since at 1414_{-23}^{+27} days, the outer planet causes negligible changes to the orbits of the inner planets on the timescale of the *Kepler* baseline. Therefore, the outer planet was only detected in RVs. The RV-led discovery highlights the importance of multi-method follow-up of the most architecturally interesting *Kepler* planetary systems.

6.3. Architectural constraints from photodynamical modeling

From the photodynamical analysis, we determined that the two inner planets, b and c, are apsidally anti-aligned. Our result agrees with N13, who also found that planets b and c are ap-

sidally anti-aligned. Apsidal anti-alignment is a predicted outcome of convergent or divergent Type I migration in a viscous disk (Nelson 2018, and references therein). The combination of the near-resonant configuration for the inner planets and their apsidal anti-alignment suggests a history of migration and resonant trapping.

Planet d’s longitude of periastron passage is nearly aligned with that of planet b, and anti-aligned with that of planet c. The apsidal alignment of planet d is far less meaningful, since it is dynamically decoupled from the inner two planets. However, the eccentricity of planet d is large ($e_d = 0.432 \pm 0.048$) compared to the inner planets ($e_{b,c} \approx 0.06$). The high eccentricity

Table 5. Phodymm MCMC Posteriors

Parameter	Units	Median $\pm 1\sigma$
Period _b	days	10.91647 ^{+0.00015} _{-0.00013}
T _{0,b}	BJD–BJD ₀	55.0807 ^{+0.0006} _{-0.0006}
$\sqrt{e} \cos \omega_b$		0.23576 ^{+0.00032} _{-0.00031}
$\sqrt{e} \sin \omega_b$		0.0045 ^{+0.0028} _{-0.0027}
<i>i</i> _b	°	90.97 ^{+0.12} _{-0.12}
M _{jup,b}	Jup	0.0299 ^{+0.0036} _{-0.0037}
R _b /R _s		0.03515 ^{+0.00018} _{-0.00018}
Period _c	days	22.2649 ^{+0.00068} _{-0.00067}
T _{0,c}	BJD–BJD ₀	61.354 ^{+0.026} _{-0.025}
$\sqrt{e} \cos \omega_c$		0.23919 ^{+0.00087} _{-0.00107}
$\sqrt{e} \sin \omega_c$		0.0046 ^{+0.0033} _{-0.0035}
<i>i</i> _c	°	93.14 ^{+0.68} _{-0.69}
Ω _c	°	0.43 ^{+0.18} _{-0.21}
M _{jup,c}	Jup	0.674 ^{+0.017} _{-0.016}
Period _d	days	1414.0 ^{+27.0} _{-23.0}
T _{0,d}	BJD–BJD ₀	1323.0 ^{+30.0} _{-33.0}
$\sqrt{e} \cos \omega_d$		0.641 ^{+0.031} _{-0.034}
$\sqrt{e} \sin \omega_d$		0.09 ^{+0.057} _{-0.053}
M _{jup,d}	Jup	3.02 ^{+0.19} _{-0.18}
M _s	solar	0.99 ^{+0.024} _{-0.023}
R _s	solar	0.897 ^{+0.016} _{-0.016}
<i>c</i> ₁		0.395 ^{+0.061} _{-0.062}
<i>c</i> ₂		0.291 ^{+0.097} _{-0.095}
σ _b	m/s	7.0 ^{+1.04} _{-0.87}
σ _c	m/s	8.2 ^{+5.6} _{-4.9}
M _b	Earth	9.5 ^{+1.2} _{-1.2}
M _c	Earth	214.2 ^{+5.4} _{-5.0}
M _d	Earth	959.0 ^{+59.0} _{-56.0}
R _b	Earth	3.438 ^{+0.076} _{-0.074}
ρ _b		1.29 ^{+0.16} _{-0.16}
<i>e</i> _b		0.05561 ^{+0.00013} _{-0.00013}
<i>e</i> _c		0.05724 ^{+0.00041} _{-0.00049}
<i>e</i> _d		0.422 ^{+0.039} _{-0.041}
T _{p,d}	BJD	2455868.99621109

NOTE—The MCMC parameters are above the line; derived parameters are below the line. All parameters are computed at epoch $T_{0,\text{BJD}} = 2454954.62702$. Ω_b is an arbitrary reference angle and was fixed at 0.0. The Photodynamical solution was not sensitive to the inclination of planet d, which we fixed at $i_d = 89^\circ$.

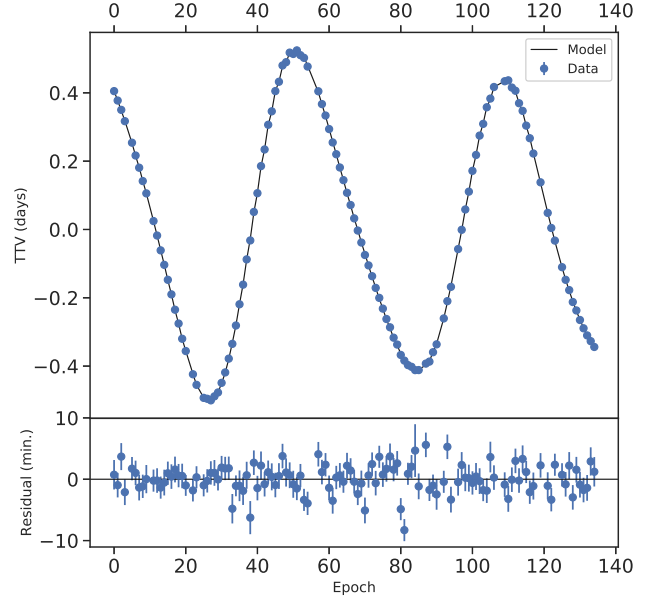


Figure 5. Top: The Kepler-88 b TTVs from the Kepler long-cadence lightcurves (blue, [Holczer et al. 2016](#)), and our best N-body, 3-planet model to the TTVs and RVs (black). Bottom: The residuals.

of planet d could be explained by planet-planet scattering or high-eccentricity migration in the past. By contrast, the modest eccentricities of planets b and c could possibly be explained by the equilibrium of disk and/or tidal circularization and N-body eccentricity pumping.

We find that the mutual inclination of planets b and c is tightly constrained: $i_b = 90.97 \pm 0.11^\circ$, and $i_c = 93.14 \pm 0.68^\circ$. This is in agreement with N13, who found $95^\circ < i_c < 98^\circ$.⁵ To test the extent to which the inclinations of the planets are constrained photodynamically, we initialized a DE-MCMC experiment with 40 walkers with our best fit, but flipped the inclination of planet c about the stellar meridian ($i = 90^\circ$), allowing the same parameters to vary as in our

⁵ Note that the N13 definition of inclination was based on planets transiting at $i = 0$; we have converted their measurements to the planet-transit at $i = 90^\circ$ coordinate system.

Table 6. Kepler-88 b Transit Times and Velocities

Epoch	Transit Mid-time (BJD–BJD ₀)	Impact Parameter (AU)	Transit Velocity (AU/day)
0	5.508030969594398840e+01	2.0577992101e-03	5.4311191447e-02
1	6.600700748081904123e+01	2.0554661003e-03	5.4351568806e-02
2	7.692950623747276495e+01	2.0538053465e-03	5.4507551040e-02
3	8.785353516418138042e+01	2.0507331523e-03	5.4561198558e-02
4	9.877232802144204982e+01	2.0486979666e-03	5.4710854735e-02
5	1.096938973538097315e+02	2.0449774489e-03	5.4777039310e-02

NOTE—BJD₀ = 2454900. The full table is available in machine readable form. The first few lines are shown here for content and format.

control trial. In general, it is difficult for a DE-MCMC exploration to find this parameter space, because inclinations near 90° for planet c would produce deep transits, which are not observed. However, our inclination-flipped experiment performed substantially worse than our best fit, with $\Delta\text{BIC} = 35$ (see Table 4). Therefore, our findings strongly disfavor the model in which planets b and c are on opposite sides of the star; rather, they seem to be on the same side of the star, and with a mutual inclination of $1.88 \pm 0.69^\circ$.

Constraints on the mutual inclinations of planets likely come from transit duration variations (TDVs). The best-fit solution to our photodynamical model includes substantial TDVs for planet b (see Figure 10), though these are dominated by midplane precession (i.e., Nesvorný et al. 2013). We determined the TDVs based on the velocities and impact parameters in Table 6:

$$T_{i,\text{dur}} = \frac{2\sqrt{\left(\frac{R_\star}{\text{au}}\right)^2 - \left(\frac{b_i}{\text{au}}\right)^2}}{v_{i,\text{pl}} \times \text{day/au}} \text{days} \quad (4)$$

where R_\star/au is the stellar radius in units of au, b_i is the i^{th} transit impact parameter in units of au, and $v_{i,\text{pl}}$ is the velocity of the planet during the i^{th} transit in units of au/day.

We explored the extent to which we could constrain the inclination of planet d from the TTVs. By keeping $M \sin i_d$ constant but varying i_d and M_d , we found that the best-fit solution to the TTVs did not significantly degrade. We tried this experiment in forward-modeling the TTVs with `TTVFast` and also with `Phodymm`. In both cases, a wide range of mutual inclinations between planet d and the inner planetary system are supported by the data. For example, fixing the inclination of planet d to be nearly perpendicular to the inner planets ($i_d = 30^\circ$) only increased (worsened) the BIC of our photodynamical model by 5, which suggests only modestly better performance of a coplanar model. However, we have not examined the long-term orbital stability of solutions where planet d is highly inclined with respect to the inner system. Simulations in similar planetary systems have found that a long-period giant planet is likely to be coplanar with the inner planets, as this configuration is usually stable for longer periods of time than highly mutually inclined geometries (Becker & Adams 2017). In an analysis of the Kepler-88 system, Denham et al. (2019) found that a planet at semi-major axis 2.4 au with $e = 0.432 \pm 0.048$ would be stable so long as its mass was $< 20M_J$. At $M \sin i_d = 959 \pm 57 M_\oplus$,

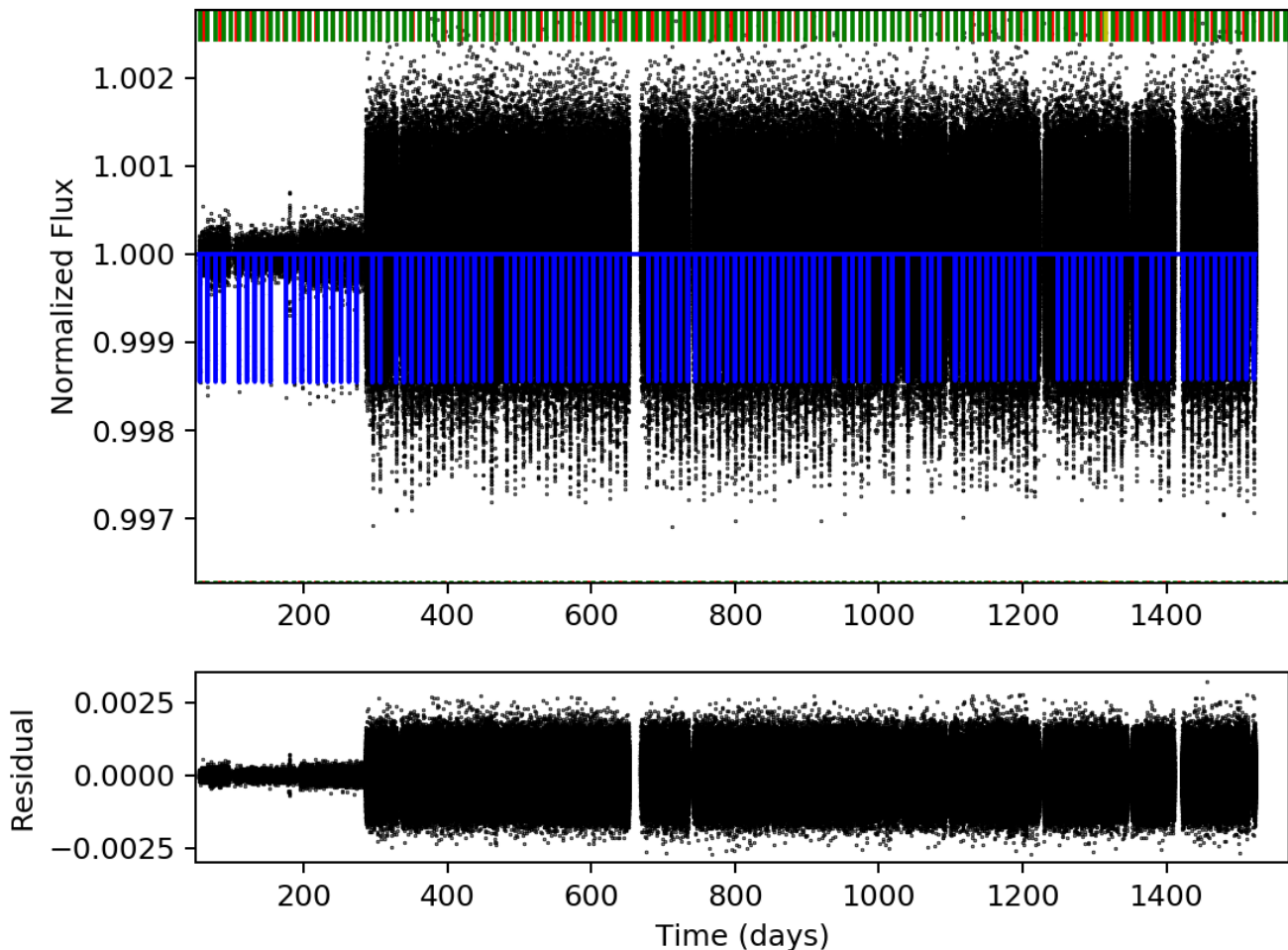


Figure 6. Top: The detrended, flux-normalized, Q1-Q17 lightcurves of Kepler-88 (black points), as a function of days in BJD-2454900. Photometry from before day ~ 300 are from Kepler’s long-cadence mode, whereas later photometry are from Kepler’s short-cadence mode. The best-fit photodynamical model is overplotted in blue. The conjunction times of planets b (red), c (green), and d (yellow) are marked. Note that planets c and d do not transit. Bottom: The residuals.

Kepler-88 b could take on a range of inclinations without disrupting the inner system.

6.4. Long-term Evolution

The architecture of a long-period giant planet accompanying two closer-in planets reminded us of the Kepler-56 system. Kepler-56 is a red giant star hosting two coplanar, transiting planets whose orbits are misaligned with respect to the stellar rotation axis, which is determined from the asteroseismic modes of the star (Huber et al. 2013). Radial velocity monitoring of the system revealed a long-period, non-transiting giant

planet with moderate eccentricity (Otor et al. 2016). Follow-up theoretical work (Gratia & Fabrycky 2017) suggested that the outer planet can become eccentric due to planet-planet scattering. In such cases, additional outer planet(s) are likely ejected, leaving the surviving outer planet on an eccentric and inclined orbit. The perturbations ripple to the inner system, not necessarily disrupting it, but possibly causing precession of the orbital plane that periodically

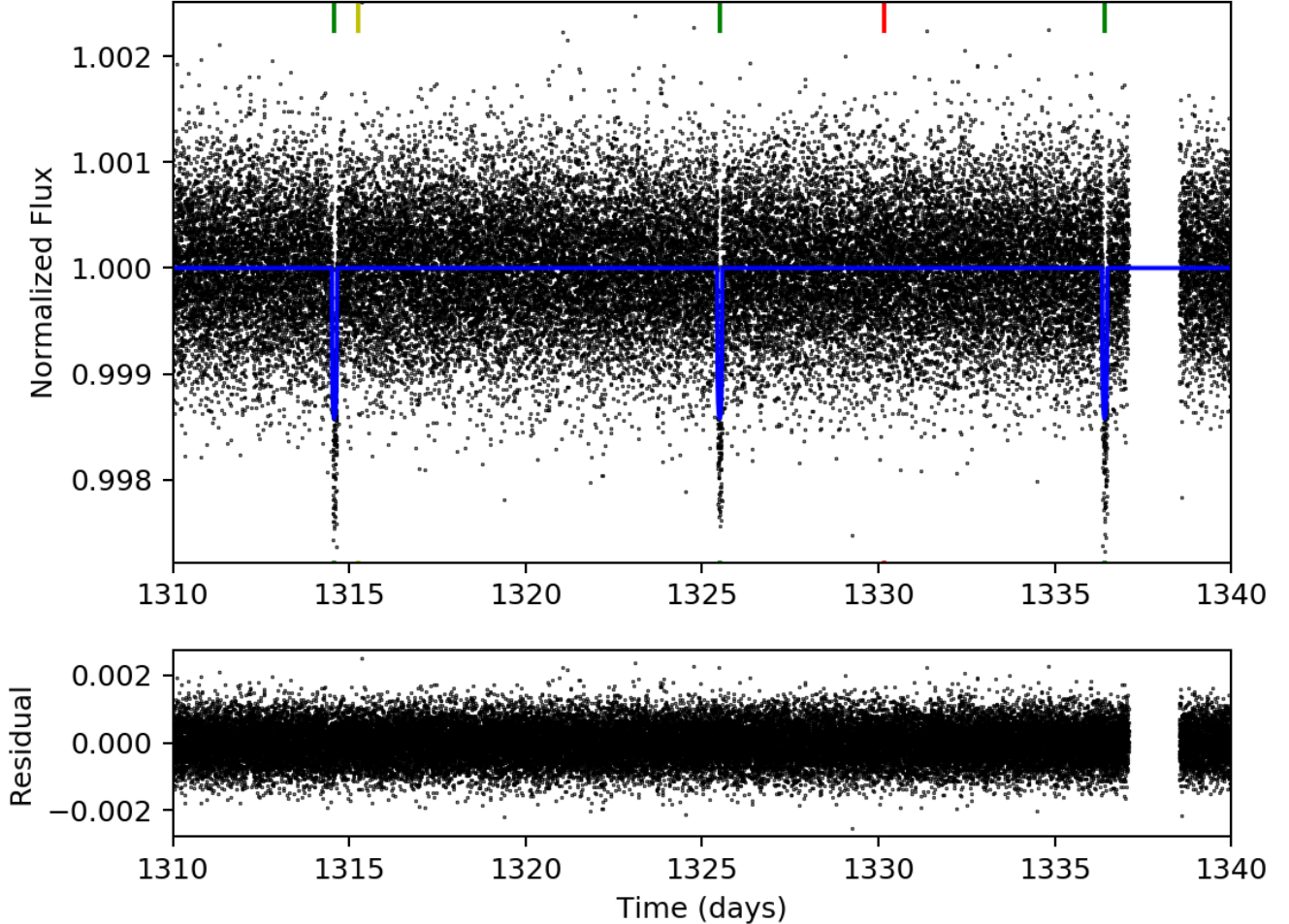


Figure 7. A zoomed in version of Figure 6. The green ticks indicate transits of planet b, the red tick is a (non-transiting) conjunction of planet c, and the yellow tick is (non-transiting) conjunction of planet d. There is no evidence for transits of planets c or d.

misaligns those two planets from the host star’s equatorial plane.⁶

Here we run a long-term N-body simulation for Kepler-88 to observe the evolution. For the simulation we entered a fit of the data into the Mercury package (Chambers 1999) and used the Burlisch-Stoer integrator for 0.1 Myr to record the secular-timescale effects. We have assumed the outer planet is inclined 30 degrees to the inner planets, but that is not constrained from the

data. In Figure 11 we show that no substantial eccentricity is transferred from the outer giant to the inner planets on these timescales, but a long-term precession effect can excite the inner planets to a large inclination relative to the star. In contrast, the orbital planes of the two inner planets remain closely aligned to each other.

We follow Boué & Fabrycky (2014) to evaluate the secular timescales. The frequency at which the inner planets would precess due to the outer planet, if the outer planet were not to back-react, is $\nu_3 = 2.7 \times 10^{-12} \text{ rad s}^{-1}$ (74 kyr period). The frequency that the outer planet would precess due to the inner planets, if they were not to

⁶ For the Kepler-88 system, another possible consequence could be to leave the resonant libration in an excited state, accounting for the large TTVs.

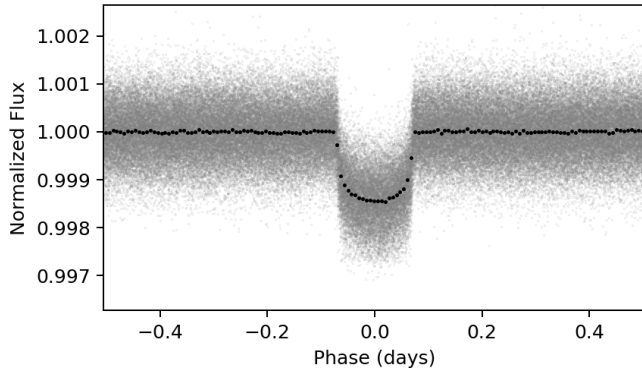


Figure 8. The photometry from Figure 6 (gray) has been phase-folded to the best-fit times of conjunction of planet b, with conjunction times determined by our photodynamical model (the blue model in Figure 6). The black points are a running median to more clearly show the transit shape. The transit ingress and egress are sharp, with no evidence of horizontal smearing from improperly determined transit times. There are no detected transits of planets c or d.

back-react, is $\nu_4 = 1.5 \times 10^{-13} \text{ rad s}^{-1}$ (1.33 Myr period). Together, the frequency of precession should be $\nu = \cos(i)(\nu_3 + \nu_4) = 2.5 \times 10^{-13} \text{ rad s}^{-1}$ (81-kyr period). The frequencies related to stellar spin precession are several orders of magnitude smaller. Therefore the inner planets are effectively precessing due to the outer planet, without much back-reaction (as is evident also Figure 11, with a precessional frequency of 77 kyr, near the analytic value), and the star’s precession cannot keep up with that relatively quick motion. So we expect that a spin orientation measurement of the star, with respect to the transiting planet’s orbit, would help diagnose whether the outer planet has a significant inclination with respect to the inner planets.

7. DISCUSSION

7.1. Implications for planet formation

Since both planets c and d are gas giants, they must have formed early in the disk lifetime, when gas was abundant. The presence of multi-

ple giant planets in this system is unsurprising since $[\text{Fe}/\text{H}] = 0.27 \pm 0.06$, and the occurrence of giant planets increases with stellar metallicity (Fischer & Valenti 2005). Perhaps additional giant planets were present earlier, or are still present. Planets c and d likely underwent viscous (Type I) migration in the proto-planetary disk. As the gas disk dissipated, planet-planet scattering would likely have increased, and low- and high-eccentricity migration likely became important at this time. The high eccentricity of planet d probably arose due to a significant exchange of angular momentum with another gas-giant planet.

The formation of planet b could have been contemporaneous with the giant planets if the planet were somehow gas-starved, resulting in only a low-mass volatile envelope. Or perhaps planet b formed when gas was less abundant and was caught in mean motion resonance with planet c during an epoch of inward migration of planet c.

7.2. Comparison to Other Planetary Systems

Giant planets are present around a large number of the *Kepler* systems that host small, transiting planets (Marcy et al. 2014; Mills et al. 2019), and perhaps at greater frequency than giant planets occur around field stars (Zhu & Wu 2018; Bryan et al. 2019). Kepler-88 joins their ranks. Furthermore, Kepler-88 has two giant planets. Other systems with multiple giant planets in addition to small transiting planets include WASP-47 (Neveu-VanMalle et al. 2016) and 55 Cnc (McArthur et al. 2004). The stellar and planetary properties of these systems are summarized in Table 7.

Like Kepler-88, WASP-47 has a nearly-circular hot Jupiter and a slightly eccentric longer-period giant planet (Sinukoff et al. 2017; Weiss et al. 2017; Vanderburg et al. 2017). Similarly, 55 Cnc has a close-in, nearly circular warm Jupiter at $P = 14.7$ days, and three other known giant planets at 44.4, 261, and 4800 days

Table 7. Systems with Multiple Giant Planets and Small Transiting Planets

Parameter	Units	Kepler-88	55 Cnc	WASP-47
Stellar Parameters				
T_{eff}	K	5466 ± 60	5196 ± 24	5552 ± 75
M_{\star}	M_{\odot}	0.985 ± 0.024	0.905 ± 0.015	1.040 ± 0.031
R_{\star}	R_{\odot}	0.900 ± 0.022	0.943 ± 0.010	1.137 ± 0.013
[Fe/H]	dex	0.27 ± 0.06	0.31 ± 0.04	0.38 ± 0.05
Age	Gyr	1.9 ± 1.6	10.2 ± 2.5	6.5 ± 2
Innermost Transiting Planet				
Letter		b	e	e
Period	days	10.91649 ± 0.00014	0.736539 ± 0.000007	0.789592 ± 0.000012
R_{p}	R_{\oplus}	3.563 ± 0.09	1.91 ± 0.08	1.810 ± 0.027
M_{p}	M_{\oplus}	9.1 ± 1.1	8.08 ± 0.31	6.83 ± 0.66
ρ_{p}	g cm^{-3}	1.11 ± 0.15	6.4 ± 0.8	6.35 ± 0.64
Innermost Giant Planet				
Letter		c	b	b
Period	days	22.26494 ± 0.0007	14.65152 ± 0.00015	4.1591289 ± 0.0000042
$M \sin i$	M_{\oplus}	200.5 ± 2.9	264.0 ± 1.0	363.1 ± 7.3
Ecc.		0.05734 ± 0.0004	0.0034 ± 0.0032	< 0.002
Outermost Known Giant Planet				
Letter		d	d	c
Period	days	1431^{+59}_{-40}	4825 ± 39	588.5 ± 2.4
$M \sin i$	M_{\oplus}	918 ± 57	1232 ± 22	398.2 ± 9.3
Ecc.		0.432 ± 0.048	0.019 ± 0.013	0.296 ± 0.017

NOTE—For Kepler-88: stellar parameters are from [Fulton & Petigura \(2018\)](#), and planetary parameters are from this work. For 55 Cnc: stellar parameters are from [von Braun et al. \(2011\)](#), and planetary parameters are from [Demory et al. \(2016, planet e\)](#) and [Baluev \(2015, other planets\)](#). For WASP-47: stellar and planetary parameters are from [Vanderburg et al. \(2017\)](#).

([Marcy et al. 2002](#); [Naef et al. 2004](#); [McArthur et al. 2004](#); [Fischer et al. 2008](#); [Wright et al. 2009](#); [Dawson & Fabrycky 2010](#); [Endl et al. 2012](#); [Nelson et al. 2014](#); [Baluev 2015](#)). In general, systems with hot Jupiters do not tend to have companions within ~ 5 au ([Steffen et al. 2012b](#); [Bryan et al. 2016](#)), but perhaps systems with hot/warm Jupiters in proximity to small exoplanets and/or with metal-rich stars are an

exception. Long-baseline RV studies of the Kepler and TESS systems with hot and/or warm Jupiters in addition to small planets will reveal whether these systems also have distant giant planets.

Kepler-88 differs from 55 Cnc and WASP-47 in that the innermost known planet has an orbital period of 11 days, rather than < 1 day. Both 55 Cnc e and WASP-47 e are examples of

“ultra-short period” (USP) planets, which are defined as having $P < 1$ day (Dawson & Fabrycky 2010; Becker et al. 2015). USPs are generally small ($R_p < 2 R_\oplus$ Sanchis-Ojeda et al. 2014); this is likely because their high equilibrium temperatures do not support a volatile envelope of hydrogen and helium, although they could support thin envelopes of heavier mean molecular weight species like water or silicates (Lopez 2016). Kepler-88 b is nearly the size of Neptune, and, at a density of 1.1 g cm^{-3} , has abundant hydrogen and helium. However, its mass of $9.5 \pm 1.2 M_\oplus$ is very similar to the masses of 55 Cnc e and WASP-47 e. Perhaps the nearby giant planet will eventually perturb Kepler-88 b into an orbit with $P < 1$ day, where photo-evaporation would remove the H/He envelope. Kepler-88 is significantly younger than the other systems (age = 1.8 ± 1.6 Gyr, see Table 7). Thus, Kepler-88 might represent an early prototype of the 55 Cnc and WASP-47 systems.

7.3. Comparison of RV and TTV Masses

The measurement of planetary masses with radial velocity and transit timing may always be confused by the presence of additional planets perturbing the star (RV) or the transiting planet(s) (TTVs). In addition, both techniques can suffer from stellar systematics such as stellar jitter (RV) or stellar photometric inhomogeneities (TTVs), as well as instrumental systematics. This motivates a comparison of these two techniques when both are available. Unfortunately the number of systems for which this is possible is very small in number due to the small probability of transit of RV-detected systems, and the poor RV precision of most TTV systems found with Kepler. Mills & Mazeh (2017) found only nine planets which had both RV and TTV mass measurements, of which eight agree to better than $2\text{-}\sigma$, while one (Kepler-89d) may be influenced by the presence of additional undiagnosed planets (Mayo et al. 2017). Note that each technique has a slightly

different dependence upon the stellar mass, so that precise stellar parameters are needed to carry out a comparison.

The Kepler-88 system adds another planet for which both RV and TTV measurements are available: Kepler-88c. In our RV analysis, we found a minimum mass of this planet of $M_c \sin i_c = 0.67 \pm 0.033 M_J$, while in an analysis of the TTVs only using a three-planet model we found a best-fit mass of $M_c = 0.685 M_J$. The photodynamical analysis indicates an inclination for planet c of 93.14 degrees, so these two determinations agree to within $1 - \sigma$. Thus, Kepler-88c adds to the number of cases in which a consistent RV and TTV mass are obtained, building confidence in both techniques. A more detailed discussion of the information content of the RVs vs. TTVs is in the Appendix.

7.4. Opportunities for future observation

The presence of two planets in near-resonant orbits can sometimes be confused for a single planet with moderate eccentricity (Wittenmyer et al. 2019). Our RV baseline is too short, and our sampling of the periastron too sparse, to fully explore the possibility of a fourth planet in the system (see Figure 9). Future RV monitoring, especially during the expected periastron passage of planet d, will refine the orbit of planet d and might place constraints on the possibility of a fourth planet. Based on the $2\text{-}\sigma$ uncertainties in the orbital period, the next periastron passage of planet d will occur between 2019 November and 2020 June.

The TESS spacecraft observed Kepler-88 during its northern hemisphere campaign this summer. The photometric precision of TESS should be adequate to detect Kepler-88 b, if the planet is still transiting (Christ et al. 2018).

8. CONCLUSION

With six years of radial velocity monitoring, we have confirmed the presence, orbit, and mass of the giant planet Kepler-88 c: $P_c =$

22.2649 ± 0.0007 days, $M_c = 214.2 \pm 5.2 M_\oplus$. This giant planet perturbs the orbit of the transiting planet Kepler-88 b and produces its TTVs. We have also discovered an additional giant planet, Kepler-88 d, in an orbital period of $P_d = 1414_{-23}^{+27}$ days with moderate eccentricity $e_d = 0.432 \pm 0.048$ and mass $M \sin i_d = 959 \pm 57 M_\oplus$. Our analysis of the RVs only versus a full photodynamical model demonstrated that the RVs were necessary to detect planet d, but that the orbits and masses of planets b and c are much better determined with a full photodynamical model than with RVs alone. Both techniques independently give consistent values for the mass of planet c. Kepler-88 joins the ranks of metal-rich stars that host both small transiting planets and two or more giant planets.

ACKNOWLEDGMENTS

LMW thanks Molly Kosiarek, Ian Crossfield, Sarah Blunt, Lee Rosenthal, Sam Grunblatt, and Ryan Rubenzahl for contributing to the collection of Keck-HIRES RVs, and Dan Foreman-Mackey and Ben Montet for useful discussions. LMW acknowledges the support of Ken & Gloria Levy, the Trottier Family Foundation, and the Beatrice Watson Parrent Fellowship. EA acknowledges support from NSF grant AST-1615315, NASA grants NNX13AF62G, NNA13AA93A and 80NSSC18K0829. Kepler was competitively selected as the tenth NASA Discovery mission. Funding for this mission is provided by the NASA Science Mission Directorate. We are grateful to the time assignment committees of the University of California, the University of Hawaii, and NASA for allocating observing time to complete this multi-year project. This work benefited from the 2017 Exoplanet Summer Program in the Other Worlds Laboratory (OWL) at the University of California, Santa Cruz, a program funded by the Heising-Simons Foundation. This research was partially conducted during the Exostar19 program at the Kavli Institute for Theoretical Physics at UC Santa Barbara, which was supported in part by the National Science Foundation under Grant No. NSF PHY-1748958.

The authors wish to recognize and acknowledge the very significant cultural role and reverence that the summit of Mauna Kea has always had within the indigenous Hawaiian community. We are most fortunate to have the opportunity to conduct observations from this mountain.

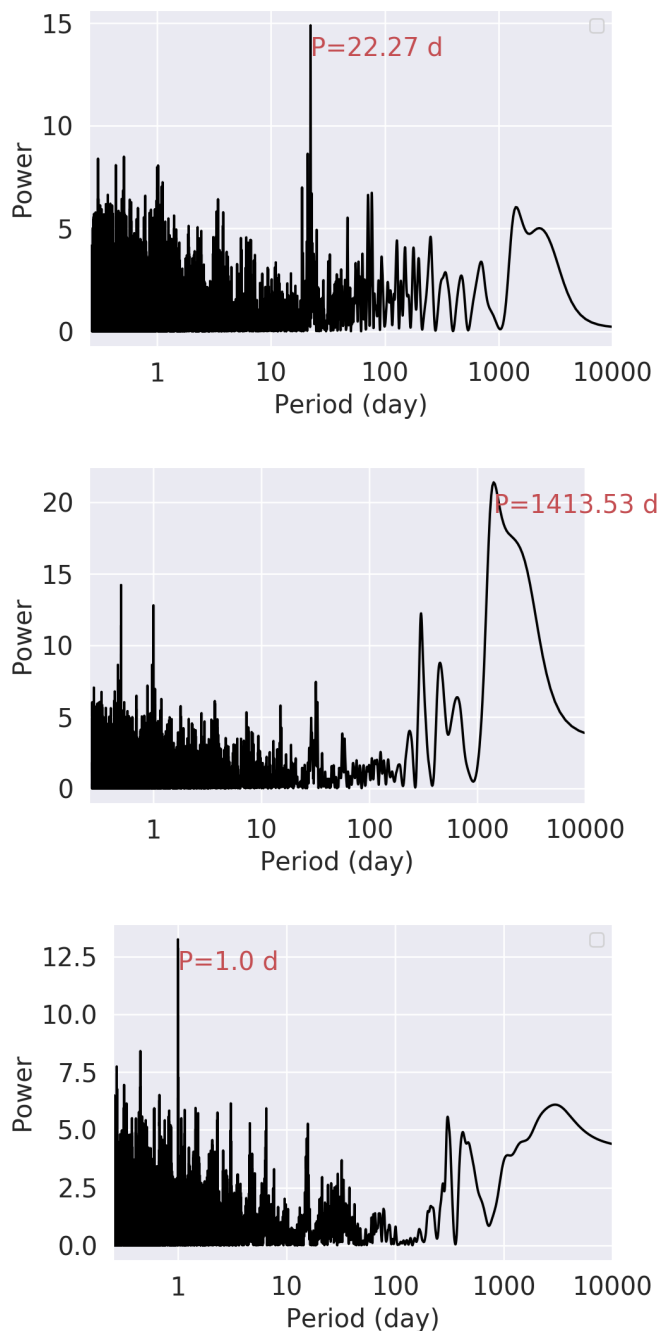


Figure 9. Top: Lomb-scargle periodogram of the Kepler-88 RVs. Middle: Lomb-scargle periodogram to the residual RVs, after subtracting the best-fit N-body two-planet model (planets b & c). The significant peak at 1400 days is strong evidence for a third planet in the system. Bottom: Lomb-scargle periodogram to the residual RVs, after subtracting the best N-body three-planet model. There is a strong peak at 1.0 days that is likely the consequence of correlated noise and our window function. If there is a fourth planet, its orbital period is not yet apparent.

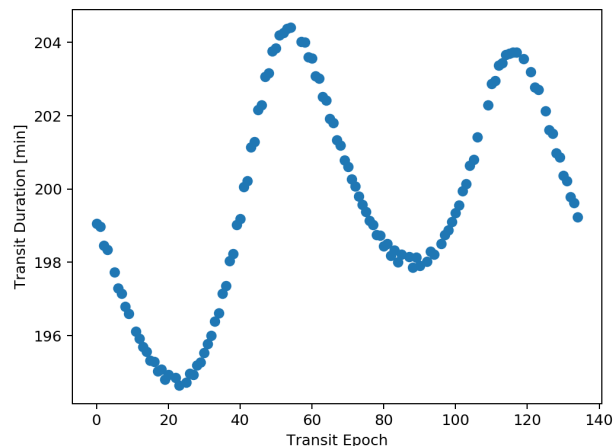


Figure 10. The best-fit durations of the individual transits from our photodynamical model.

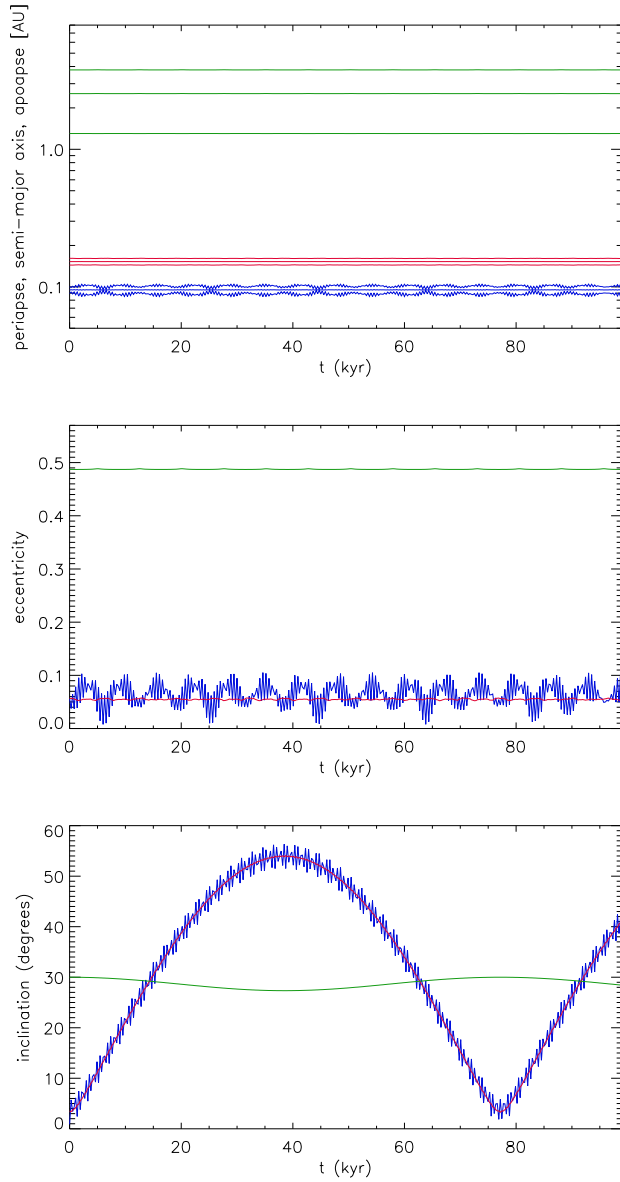


Figure 11. Long-term dynamical simulation of the system. Planets b, c, and d are represented in blue, red, and green respectively. Top panel: the semi-major axis, periapse distance, and apoapse distance for each planet, as a function of time. Middle panel: Planetary eccentricities. Bottom panel: Inclination to a plane formed by (a) the line of sight and (b) the line of intersection of planet b’s initial orbital plane and the sky plane. Over thousands of years, the orbital plane of the inner planets may be torqued through a large angle, away from the transiting configuration. Note that i_d is unknown.

REFERENCES

- Agol, E., & Fabrycky, D. C. 2018, in Handbook of Exoplanets (Springer International Publishing), 797–816, doi: [10.1007/978-3-319-55333-7_7](https://doi.org/10.1007/978-3-319-55333-7_7)
- Baluev, R. V. 2015, MNRAS, 446, 1493, doi: [10.1093/mnras/stu2150](https://doi.org/10.1093/mnras/stu2150)
- Barros, S. C. C., Díaz, R. F., Santerne, A., et al. 2014, A&A, 1, 1
- Becker, J. C., & Adams, F. C. 2017, MNRAS, 468, 549, doi: [10.1093/mnras/stx461](https://doi.org/10.1093/mnras/stx461)
- Becker, J. C., Vanderburg, A., Adams, F. C., Rappaport, S. A., & Schwengeler, H. M. 2015, ApJL, 812, L18, doi: [10.1088/2041-8205/812/2/L18](https://doi.org/10.1088/2041-8205/812/2/L18)
- Boué, G., & Fabrycky, D. C. 2014, ApJ, 789, 111, doi: [10.1088/0004-637X/789/2/111](https://doi.org/10.1088/0004-637X/789/2/111)
- Bryan, M. L., Knutson, H. A., Lee, E. J., et al. 2019, AJ, 157, 52, doi: [10.3847/1538-3881/aaf57f](https://doi.org/10.3847/1538-3881/aaf57f)
- Bryan, M. L., Knutson, H. A., Howard, A. W., et al. 2016, ApJ, 821, 89, doi: [10.3847/0004-637X/821/2/89](https://doi.org/10.3847/0004-637X/821/2/89)
- Chambers, J. E. 1999, MNRAS, 304, 793, doi: [10.1046/j.1365-8711.1999.02379.x](https://doi.org/10.1046/j.1365-8711.1999.02379.x)
- Christ, C. N., Montet, B. T., & Fabrycky, D. C. 2018, arXiv e-prints, arXiv:1810.02826. <https://arxiv.org/abs/1810.02826>
- Claret, A. 2000, A&A, 363, 1081
- Dawson, R. I., & Fabrycky, D. C. 2010, The Astrophysical Journal, 722, 937, doi: [10.1088/0004-637X/722/1/937](https://doi.org/10.1088/0004-637X/722/1/937)
- Deck, K. M., Agol, E., Holman, M. J., & Nesvorný, D. 2014, The Astrophysical Journal, 787, 132, doi: [10.1088/0004-637X/787/2/132](https://doi.org/10.1088/0004-637X/787/2/132)
- Demory, B.-O., Gillon, M., de Wit, J., et al. 2016, Nature, 532, 207, doi: [10.1038/nature17169](https://doi.org/10.1038/nature17169)
- Denham, P., Naoz, S., Hoang, B.-M., Stephan, A. P., & Farr, W. M. 2019, Monthly Notices of the Royal Astronomical Society, 482, 4146, doi: [10.1093/mnras/sty2830](https://doi.org/10.1093/mnras/sty2830)
- Endl, M., Robertson, P., Cochran, W. D., et al. 2012, The Astrophysical Journal, 759, 19, doi: [10.1088/0004-637X/759/1/19](https://doi.org/10.1088/0004-637X/759/1/19)
- Fabrycky, D. C., Lissauer, J. J., Ragozzine, D., et al. 2014, ApJ, 790, 146, doi: [10.1088/0004-637X/790/2/146](https://doi.org/10.1088/0004-637X/790/2/146)
- Fischer, D. A., & Valenti, J. 2005, ApJ, 622, 1102, doi: [10.1086/428383](https://doi.org/10.1086/428383)
- Fischer, D. A., Marcy, G. W., Butler, R. P., et al. 2008, ApJ, 675, 790, doi: [10.1086/525512](https://doi.org/10.1086/525512)
- Ford, E. B., Rowe, J. F., Fabrycky, D. C., et al. 2011, ApJS, 197, 2, doi: [10.1088/0067-0049/197/1/2](https://doi.org/10.1088/0067-0049/197/1/2)
- Fulton, B. J., & Petigura, E. A. 2018, AJ, 156, 264, doi: [10.3847/1538-3881/aae828](https://doi.org/10.3847/1538-3881/aae828)
- Gelman, A., & Rubin, D. B. 1992, Statist. Sci., 7, 457, doi: [10.1214/ss/1177011136](https://doi.org/10.1214/ss/1177011136)
- Gratia, P., & Fabrycky, D. 2017, MNRAS, 464, 1709, doi: [10.1093/mnras/stw2180](https://doi.org/10.1093/mnras/stw2180)
- Holczer, T., Mazeh, T., Nachmani, G., et al. 2016, The Astrophysical Journal Supplement Series, 225, 9, doi: [10.3847/0067-0049/225/1/9](https://doi.org/10.3847/0067-0049/225/1/9)
- Howard, A. W., & Fulton, B. J. 2016, PASP, 128, 114401, doi: [10.1088/1538-3873/128/969/114401](https://doi.org/10.1088/1538-3873/128/969/114401)
- Howard, A. W., Johnson, J. A., Marcy, G. W., et al. 2010, ApJ, 721, 1467, doi: [10.1088/0004-637X/721/2/1467](https://doi.org/10.1088/0004-637X/721/2/1467)
- Huber, D., Carter, J. A., Barbieri, M., et al. 2013, Science, 342, 331, doi: [10.1126/science.1242066](https://doi.org/10.1126/science.1242066)
- Lissauer, J. J., Ragozzine, D., Fabrycky, D. C., et al. 2011, ApJS, 197, 8, doi: [10.1088/0067-0049/197/1/8](https://doi.org/10.1088/0067-0049/197/1/8)
- Lissauer, J. J., Ragozzine, D., Fabrycky, D. C., et al. 2011, The Astrophysical Journal Supplement Series, 197, 8, doi: [10.1088/0067-0049/197/1/8](https://doi.org/10.1088/0067-0049/197/1/8)
- Lithwick, Y., Xie, J., & Wu, Y. 2012, The Astrophysical Journal, 761, 122, doi: [10.1088/0004-637X/761/2/122](https://doi.org/10.1088/0004-637X/761/2/122)
- Lopez, E. D. 2016, ArXiv e-prints. <https://arxiv.org/abs/1610.01170>
- Mandel, K., & Agol, E. 2002, ApJL, 580, L171, doi: [10.1086/345520](https://doi.org/10.1086/345520)
- Marcy, G. W., Butler, R. P., Fischer, D., et al. 2001, ApJ, 556, 296, doi: [10.1086/321552](https://doi.org/10.1086/321552)
- Marcy, G. W., Butler, R. P., Fischer, D. A., et al. 2002, ApJ, 581, 1375, doi: [10.1086/344298](https://doi.org/10.1086/344298)
- Marcy, G. W., Isaacson, H., Howard, A. W., et al. 2014, The Astrophysical Journal Supplement Series, 210, 20, doi: [10.1088/0067-0049/210/2/20](https://doi.org/10.1088/0067-0049/210/2/20)
- Mayo, A., Deck, K., Knutson, H., Batygin, K., & Christiansen, J. 2017, in American Astronomical Society Meeting Abstracts, Vol. 229, American Astronomical Society Meeting Abstracts #229, 146.32

- Mazeh, T., Nachmani, G., Holczer, T., et al. 2013, *ApJS*, 208, 16, doi: [10.1088/0067-0049/208/2/16](https://doi.org/10.1088/0067-0049/208/2/16)
- McArthur, B. E., Endl, M., Cochran, W. D., et al. 2004, *ApJL*, 614, L81, doi: [10.1086/425561](https://doi.org/10.1086/425561)
- Mills, S. M., & Fabrycky, D. C. 2017a, *ApJ*, 838, L11, doi: [10.3847/2041-8213/aa6543](https://doi.org/10.3847/2041-8213/aa6543)
- . 2017b, *AJ*, 153, 45, doi: [10.3847/1538-3881/153/1/45](https://doi.org/10.3847/1538-3881/153/1/45)
- Mills, S. M., Fabrycky, D. C., Migaszewski, C., et al. 2016, *Nature*, 533, 509, doi: [10.1038/nature17445](https://doi.org/10.1038/nature17445)
- Mills, S. M., & Mazeh, T. 2017, *The Astrophysical Journal*, 839, L8, doi: [10.3847/2041-8213/aa67eb](https://doi.org/10.3847/2041-8213/aa67eb)
- Mills, S. M., Howard, A. W., Weiss, L. M., et al. 2019, *AJ*, 157, 145, doi: [10.3847/1538-3881/ab0899](https://doi.org/10.3847/1538-3881/ab0899)
- Naef, D., Mayor, M., Beuzit, J. L., et al. 2004, *A&A*, 414, 351, doi: [10.1051/0004-6361:20034091](https://doi.org/10.1051/0004-6361:20034091)
- Nelson, B. E., Ford, E. B., Wright, J. T., et al. 2014, *MNRAS*, 441, 442, doi: [10.1093/mnras/stu450](https://doi.org/10.1093/mnras/stu450)
- Nelson, R. P. 2018, *Planetary Migration in Protoplanetary Disks*, 139, doi: [10.1007/978-3-319-55333-7_139](https://doi.org/10.1007/978-3-319-55333-7_139)
- Nesvorný, D., Kipping, D., Terrell, D., et al. 2013, *The Astrophysical Journal*, 777, 3, doi: [10.1088/0004-637X/777/1/3](https://doi.org/10.1088/0004-637X/777/1/3)
- Neveu-VanMalle, M., Queloz, D., Anderson, D. R., et al. 2016, *A&A*, 586, A93, doi: [10.1051/0004-6361/201526965](https://doi.org/10.1051/0004-6361/201526965)
- Otor, O. J., Montet, B. T., Johnson, J. A., et al. 2016, *AJ*, 152, 165, doi: [10.3847/0004-6256/152/6/165](https://doi.org/10.3847/0004-6256/152/6/165)
- Pál, A., Sárneczky, K., Szabó, G. M., et al. 2011, *MNRAS*, 413, L43, doi: [10.1111/j.1745-3933.2011.01029.x](https://doi.org/10.1111/j.1745-3933.2011.01029.x)
- Rowe, J. F., Bryson, S. T., Marcy, G. W., et al. 2014, *ApJ*, 784, 45, doi: [10.1088/0004-637X/784/1/45](https://doi.org/10.1088/0004-637X/784/1/45)
- Sanchis-Ojeda, R., Rappaport, S., Winn, J. N., et al. 2014, *ApJ*, 787, 47, doi: [10.1088/0004-637X/787/1/47](https://doi.org/10.1088/0004-637X/787/1/47)
- Sinukoff, E., Howard, A. W., Petigura, E. A., et al. 2017, *AJ*, 153, 70, doi: [10.3847/1538-3881/153/2/70](https://doi.org/10.3847/1538-3881/153/2/70)
- Steffen, J. H., Fabrycky, D. C., Ford, E. B., et al. 2012a, *MNRAS*, 421, 2342, doi: [10.1111/j.1365-2966.2012.20467.x](https://doi.org/10.1111/j.1365-2966.2012.20467.x)
- Steffen, J. H., Ragozzine, D., Fabrycky, D. C., et al. 2012b, *Proceedings of the National Academy of Science*, 109, 7982, doi: [10.1073/pnas.1120970109](https://doi.org/10.1073/pnas.1120970109)
- Vanderburg, A., Becker, J. C., Buchhave, L. A., et al. 2017, *AJ*, 154, 237, doi: [10.3847/1538-3881/aa918b](https://doi.org/10.3847/1538-3881/aa918b)
- Vogt, S. S., Allen, S. L., Bigelow, B. C., et al. 1994, in *Society of Photo-Optical Instrumentation Engineers (SPIE) Conference Series*, Vol. 2198, *Instrumentation in Astronomy VIII*, ed. D. L. Crawford & E. R. Craine, 362, doi: [10.1117/12.176725](https://doi.org/10.1117/12.176725)
- von Braun, K., Tabetha, S. B., ten Brummelaar, T. a., et al. 2011, *The Astrophysical Journal*, 740, 49, doi: [10.1088/0004-637X/740/1/49](https://doi.org/10.1088/0004-637X/740/1/49)
- Weiss, L. M., Deck, K. M., Sinukoff, E., et al. 2017, *AJ*, 153, 265, doi: [10.3847/1538-3881/aa6c29](https://doi.org/10.3847/1538-3881/aa6c29)
- Wittenmyer, R. A., Bergmann, C., Horner, J., Clark, J., & Kane, S. R. 2019, *MNRAS*, 484, 4230, doi: [10.1093/mnras/stz236](https://doi.org/10.1093/mnras/stz236)
- Wright, J. T., Upadhyay, S., Marcy, G. W., et al. 2009, *The Astrophysical Journal*, 693, 1084, doi: [10.1088/0004-637X/693/2/1084](https://doi.org/10.1088/0004-637X/693/2/1084)
- Zhu, W., & Wu, Y. 2018, *AJ*, 156, 92, doi: [10.3847/1538-3881/aad22a](https://doi.org/10.3847/1538-3881/aad22a)

APPENDIX

A. COMPARISON OF THE RVs ONLY VS. PHOTODYNAMICAL MODEL

The photodynamical fit provides some advantages over the RVs alone. Although the RV alone identifies the period of planet c as $P_c = 22.2695 \pm 0.0045$ days, the photodynamical fit tightens the uncertainty by almost an order of magnitude, finding $P_c = 22.2649 \pm 0.0007$ days. Note that the precision on our determination of the orbit of planet c is a factor of 3 better than that of N13, which found $22.3397_{-0.0018}^{+0.0021}$ days; the improvement in the precision of the orbital period must come from the additional *Kepler* photometry in our analysis, since the RVs alone did not determine the orbit of planet c as precisely as the TTV-based N13 work. Also, the RVs are only able to provide a mass upper limit for planet b, but the planet’s period, radius, and mass are determined with high confidence in the photodynamical analysis: $P_b = 10.91647 \pm 0.00014$ days (at epoch BJD= 2454954.62702), $R_b = 3.438 \pm 0.075 R_\oplus$, $M_b = 9.5 \pm 1.2 M_\oplus$. The superior performance of the photodynamical model illustrates the complementary nature of transit photometry and radial velocities: together, these techniques reveal more about the 3D architecture of a planetary system than each of these techniques does alone.

The superior mass determination of planets b and c in the photodynamical model can be traced to the chopping signal in the TTVs. In systems that are not very close to resonance and/or have large TTV uncertainties compared to the timing precision, only the low-frequency TTV super-period is detected. This low-frequency signal contains information about the mass ratio of the planets, but the absolute masses are degenerate with the eccentricities of the planets (Lithwick et al. 2012). However, in systems with high signal-to-noise TTV measurements like Kepler-88, it is possible to detect a higher-frequency signal: the synodic chopping signal. This signal abruptly changes direction after conjunctions between the transiting and perturbing planet (Agol & Fabrycky 2018). The chopping signal is therefore expected to occur at the synodic period, or

$$P_{\text{chop}} = (1/P_1 - 1/P_2)^{-1} \quad (\text{A1})$$

We identified the chopping signal in Kepler-88 by fitting the Holczer et al. (2016) TTVs with a high-order polynomial (degree 18)⁷ and subtracted this polynomial fit from the TTVs (Figure 12, upper left). The residual TTVs (lower left) show a characteristic chopping signal. Before we removed the high-degree polynomial, a Lomb-scargle periodogram of the TTVs found a periodicity of 611 days, the super-period of the TTVs (upper right). After we removed the high-degree polynomial, the Lomb Scargle periodogram of the TTV residuals had a peak at $P = 23$ days and shorter-period harmonics of that signal, which is near the expected chopping signal at 21.5 days (lower right).

⁷ We used the lowest-degree polynomial that removed significant peaks at much longer periods than the expected synodic chopping signal

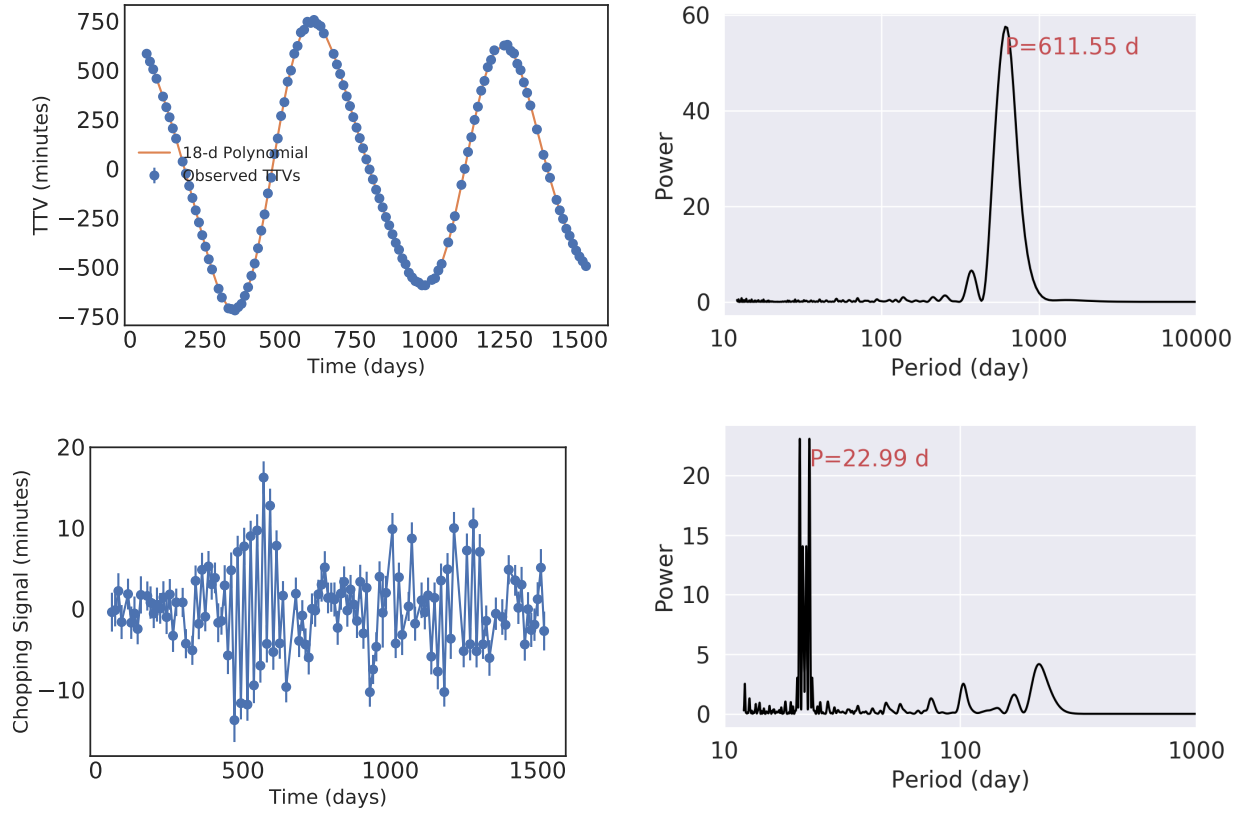


Figure 12. Determination of the Kepler-88 TTV chopping signal. Top left: The TTV signal and an 18-degree polynomial fit. Top right: The Lomb-Scargle periodogram of the TTV signal has a peak at 611 days, the super-period of the Kepler-88 TTVs. Bottom left: The high-frequency chopping signal was separated from the low-frequency TTV signal by subtracting the polynomial fit. Right: The Lomb-Scargle periodogram of the chopping signal demonstrates that low-frequency signals have been removed, and the chopping frequency of ~ 21 days is the strongest remaining frequency.